CXCR2-Expressing Tumor Cells Drive Vascular Mimicry in Antiangiogenic Therapy–Resistant Glioblastoma

Kartik Angara[*], Thaiz F. Borin[*], Mohammad H. Rashid[*], Iryna Lebedyeva[†], Roxan Ara[*], Ping-Chang Lin[*], ASM Iskander[*], Roni J. Bollag[‡], Bhagelu R. Achyut[*] and Ali S. Arbab[*]

[*]Laboratory of Tumor Angiogenesis, Georgia Cancer Center, Department of Biochemistry and Molecular Biology, Augusta University, Augusta, GA; [†]Department of Chemistry and Physics, Augusta University, Augusta, GA; [‡]Department of Pathology, Augusta University, Augusta, GA

Abstract

BACKGROUND: Glioblastoma (GBM) was shown to relapse faster and displayed therapeutic resistance to antiangiogenic therapies (AATs) through an alternative tumor cell-driven mechanism of neovascularization called vascular mimicry (VM). We identified highly upregulated interleukin 8 (IL-8)-CXCR2 axis in tumor cells in high-grade human glioma and AAT-treated orthotopic GBM tumors. *METHODS:* Human GBM tissue sections and tissue array were used to ascertain the clinical relevance of CXCR2-positive tumor cells in the formation of VM. We utilized U251 and U87 human tumor cells to understand VM in an orthotopic GBM model and AAT-mediated enhancement in VM was modeled using vatalanib (anti-VEGFR2) and avastin (anti-VEGF). Later, VM was inhibited by SB225002 (CXCR2 inhibitor) in a preclinical study. *RESULTS:* Overexpression of IL8 and CXCR2 in human datasets and histological analysis was identified as a bonafide candidate to validate VM through *in vitro* and animal model studies. AAT-treated tumors displayed a higher number of CXCR2-positive GBM-stem cells with endothelial-like phenotypes. Stable knockdown of CXCR2 expression in tumor cells led to decreased tumor growth as well as incomplete VM structures in the animal models. Similar data were obtained following SB225002 treatment. *CONCLUSIONS:* The present study suggests that tumor cell autonomous IL-8-CXCR2 pathway is instrumental in AAT-mediated resistance and VM formation in GBM. Therefore, CXCR2 can be targeted through SB225002 and can be combined with standard therapies to improve the therapeutic outcomes in clinical trials.

Neoplasia (2018) 20, 1070–1082

Precis

Therapy resistance and tumor recurrence are emerging hallmarks for several cancer types. We studied GBM as a model tumor type and AAT as a model therapeutic approach to unravel VM as an alternate neovascularization mechanism. The present study has identified the translational importance of tumor cell-autonomous IL8-CXCR2 axis-mediated mechanisms of therapy resistance, tumor recurrence, and decreased patient survival using human GBM data analysis and patient-derived and human cell line xenografts in mouse models.

Introduction

Glioblastoma (GBM) is a highly invasive, hypervascular, hypoxic, and therapy-resistant central nervous system (CNS) neoplasm with a mean survival period 1 to 3 years with the best of treatments [1].

Antiangiogenic therapy (AAT) was added as an adjuvant with the standard therapies to control the abnormal blood vessels in recurrent GBMs [2–4]. AATs targeting the endothelial cells (ECs), with lower genetic instability compared to tumors, were thought to be a viable option by blocking the vascular endothelial growth factor (VEGF)

Address all correspondence to: Ali S. Arbab, MD, PhD, Georgia Cancer Center, Augusta University, 1410 Laney Walker Blvd, CN3141, Augusta, GA 30912. E-mail: aarbab@augusta.edu

and VEGF receptor (VEGFR) pathways to counter angiogenesis without imposing drug resistance. However, the benefits of AAT were transient with refractoriness and resistance in GBM [5].

GBM-associated blood vessels are structurally different from the normal blood vessels and are more tortuous, disorganized, highly permeable, destabilized structures with abnormal endothelial and pericyte coverage, making them highly leaky and more irrigational in nature [6,7]. AAT disturbs tumor neovasculature, leading to marked hypoxia characterized by hypoxia-inducible factor 1-α (HIF-1α)–mediated upregulation of chemokine and growth factors [8]. In addition, activation of alternative pathways of neovascularization contributes to the development of AAT resistance in GBM [8–10]. It is therefore important to understand how the tumor cells coevolve to counter the AAT therapeutic insult and contribute to alternative neovascularization in GBM.

Vascular mimicry (VM) is the uncanny ability of genetically dysregulated tumor cells to transdifferentiate and acquire endothelial-like phenotypes through an intermediate stem cell–like state [11,12]. The formation of neovasculature through VM is host EC independent, classifying it as a form of vasculogenesis to mimic the function of the blood vessels [11,13–15]. Recently, we have identified VM as a major contributor to therapy-induced neovasculature in GBM models, and AAT-induced insult caused increased hypoxia, which is one of the most crucial events in the formation of VM in tumors causing resistance to AAT in GBM models [8,16,17]. Despite many studies reporting several signaling pathways involved in VM, there is a dearth of studies exploring the targetable mechanisms of AAT-induced VM in GBM. We utilized GBM as a model tumor type and AAT as a model therapeutic approach to shed light on VM as emerging mechanism of alternate neovascularization to counter the therapeutic insults.

Our previous study showed the profound role of IL-8 in an animal model of GBM [18], and blocking IL8 significantly decreased VM in tumors [8]. Recent studies have established the role of IL-8 cognate receptor CXCR2 in maintaining GBM stemness through downstream signaling pathways. These observations led us to hypothesize that IL-8-CXCR2 pathway may contribute to transdifferentiation of tumor cells into stem cell–like and endothelial cell–like phenotypes inducing VM in orthotopic GBM models. The purposes of the study are to investigate whether CXCR2-positive tumor cells are involved in the formation of VM following AAT and whether targeting IL-8-CXCR2 axis would decrease VM and GBM growth.

Materials and Methods
Details of the materials used and general methods are described in the supplemental documents.

Institutional Approval
Human GBM tissues (n = 10) were obtained from the Biorepository as paraffin-embedded tissue blocks under an institutional review board–approved protocol. For animal-based studies, the Institutional Animal Care and Use Committee and Institutional Review Board of Augusta University (protocol #2014-0625) approved all animal procedures. Body weight was measured twice weekly as an indicator of overall animal health. All efforts were made to ameliorate the suffering of animals. CO_2 with secondary method was used to euthanize animals for tissue collection at the end of the study.

Human Brain Glioma and Normal Tissue Microarray
Human Brain Glioma and Normal Tissue Microarray (GL722a) was purchased from US Biomax, Inc. The array provides a total of 63

malignant glioma samples, 10 normal cerebrum samples, and 1 pheochromocytoma as formalin-fixed, paraffin-embedded sections. These samples were stained with hCXCR2 antibody (R&D Systems, Cat# MAB331) and further processed for Periodic Acid-Schiff (PAS) staining to identify VM structures.

Human Data Analysis
The mRNA expression data for CXCR2 expression from patient's datasets classified according to the brain and CNS cancer type, recurrence status, and GBM grade were analyzed using Oncomine data (vandenBoom Brain Statistics, www.oncomine.org). Overall survival and progression-free survival Kaplan-Meier estimates were calculated by analyzing tumor samples with mRNA data (166 samples) for two genes (IL8 and CXCR2) using cBioportal platform [Glioblastoma Multiforme (TCGA, Provisional), http://www.cbioportal.org/index.do].

Cell Sorting and Immunopaired Antibody Detection Analysis
Wild-type, scrambled, and CXCR2-KD U251 cells were labeled with PerCP/Cy5.5 anti-human CD182 (CXCR2) antibody (Biolegend, Cat# 320718) and subsequently used to sort CXCR2+ and CXCR2- cells using Becton Dickinson FACSAria II SORP. Subsequently, for immune-paired antibody detection analysis by Activ Signal LLC (MA, USA), the protein lysates from scrambled, CXCR2-KD, CXCR2+, and CXCR2- U251 cells were analyzed for expression of 70 different human protein targets covering 20 major signaling pathways. The results were provided as an overview heat map for all of the samples across all of the 70 targets in the panel.

### GBM Animal Model and Treatment Groups
Tumor-bearing animals were randomly assigned to vehicle (5% DMSO + 20% sucrose solution in PBS), vatalanib (50 mg/kg/day, oral), avastin (monoclonal antibody against VEGF-A, 10 mg/kg/twice a week, IV), SB225002 (10 mg/kg/day IP), and a combination of vatalanib and SB225002 (Vata+SB) treatments (n = 3). Drug administration started 8 days after tumor implantation and continued for 2 weeks (5 days/week). Athymic nude rats were also randomly assigned to either the early (0-21 days) or delayed (8-21 days) vatalanib drug treatment or the vehicle treatment. Twenty-two days after tumor implantation, animals underwent magnetic resonance imaging (MRI) followed by euthanasia and collection of brain tissue for flow cytometry and immunohistochemical analysis. For *in vitro* studies, the doses of vatalanib and avastin were 10 μM and 100 μg/ml, respectively, and 1 μM and 2 μM of SB225002 after assessing the cell survival by MTT assay after 24 and 48 hours in U251 GBM cells in a dose range of 100 nm-4 μM (Supplementary Figure S5C).

Characterization of Tumor Cell Phenotypes
For the *in vivo* studies, freshly isolated U251 and U87 tumors were passed through a 40-μm cell strainer to make single cell suspension and incubated for 45 minutes at 4°C with 1% BSA-PBS-EDTA solution to inhibit nonspecific binding of antibodies. Flow cytometry data were acquired using Accuri C6 machine (BD Biosciences) and analyzed by BD Accuri C6 software.

Determination of IL-8 by Protein Array
Total cell lysates from snap frozen brains containing tumor treated with vehicle and vatalanib were processed for customized human cytokine array (40 factors) (Ray Biotech) including IL-8 as per the manufacturer's protocol. Membranes were imaged using LAS-3000 system (Fuji Film,
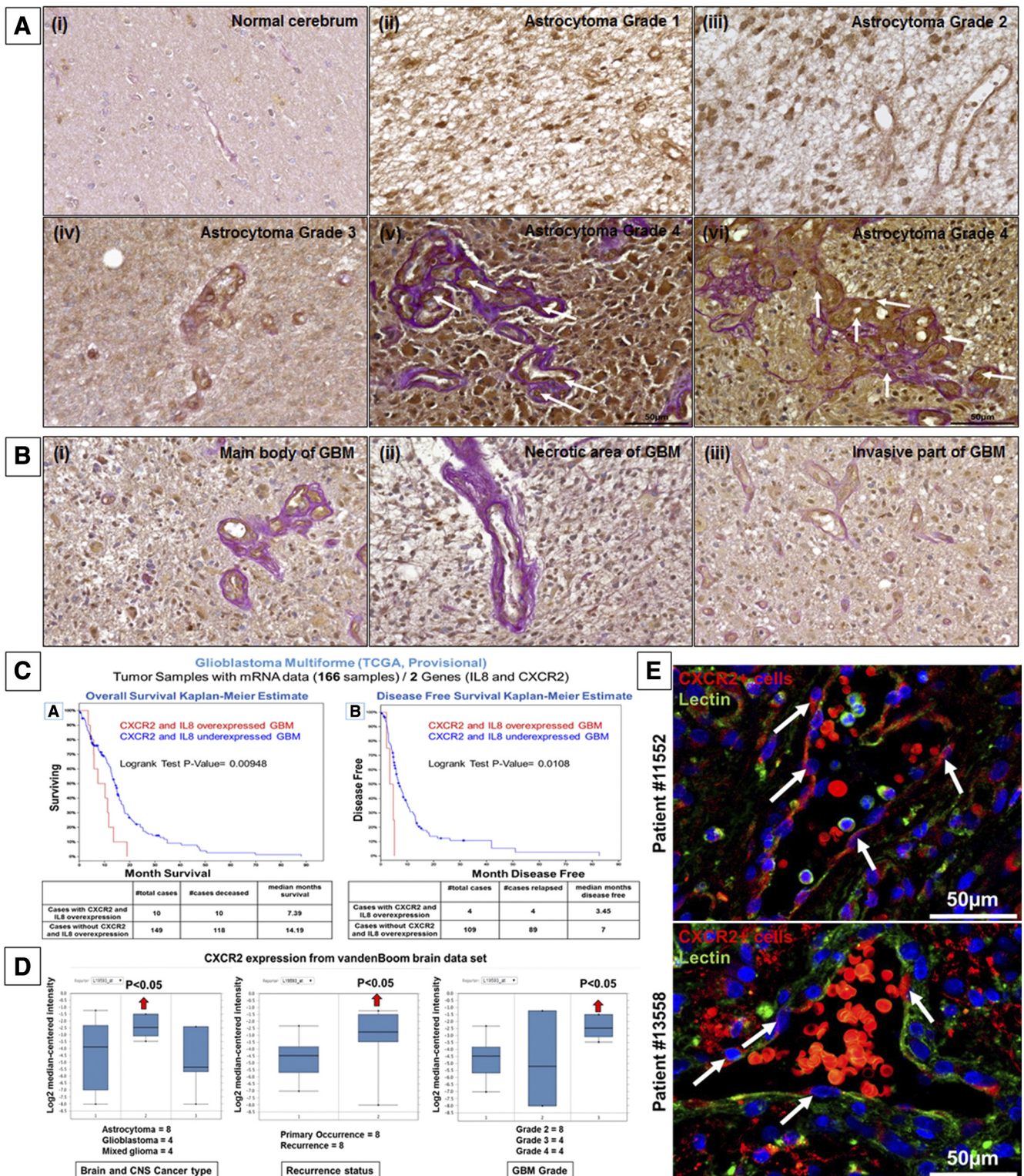
Figure 1. CXCR2+ tumor cells line PAS-positive VM structures in human GBM samples and positively correlate with recurrence and grade of GBM. (A) CXCR2+ GBM cells lining the PAS-positive VM structures in normal cerebrum (i) and different grades of GBM (grade 1-ii, grade 2-iii, grade 3-iv, and grade 4-v and vi). (B) CXCR2+ cells lining PAS-positive VM structures in different areas of GBM tissue, the main body of GBM (i), the part of the GBM tissue next to necrotic area (ii), and the invasive part of GBM (iii). (C) TCGA brain data analyzed for IL-8 and CXCR2 genes to assess the overall survival and disease-free survival as a Kaplan-Meier estimate. (D) Oncomine data analysis of the different gliomas according to brain and CNS cancer type, recurrence status, and GBM grade. (E) CXCR2+ GBM cells represented by red color (white arrows) lining the VM structures carrying functional red blood cells (circular RBCs auto fluorescence in red color), thereby demonstrating the functional nature of these VM structures. Lectin (green) shows the lining of the functional vessels.

Japan). The expression intensity emitted from the membrane was normalized to the positive control spots of the corresponding membrane using Image J software.

Immunohistochemistry and Immunofluorescence

The sections were double stained for CXCR2 expression followed by PAS, according to the protocols of the suppliers of primary antibodies. For immunofluorescence visualization of CXCR2+ tumor cells in forming VM, the slides were incubated with anti-CXCR2 and anti-Laminin antibody overnight at 4°C. The following day, slides were washed, stained with Rhodamine-red/TRITC-conjugated or FITC-conjugated secondary antibodies (1:100), counterstained with DAPI, and then mounted using Vectashield (Vector Laboratories, Burlingame, CA). The images were acquired using an automated all-in-one microscope (BZ-X710, Keyence).

Tube Formation Assay

A total of 2×10^4 U251 and U87 GBM cells were seeded into a 96-well plate precoated with 50 µl of Matrigel (Corning, Cat
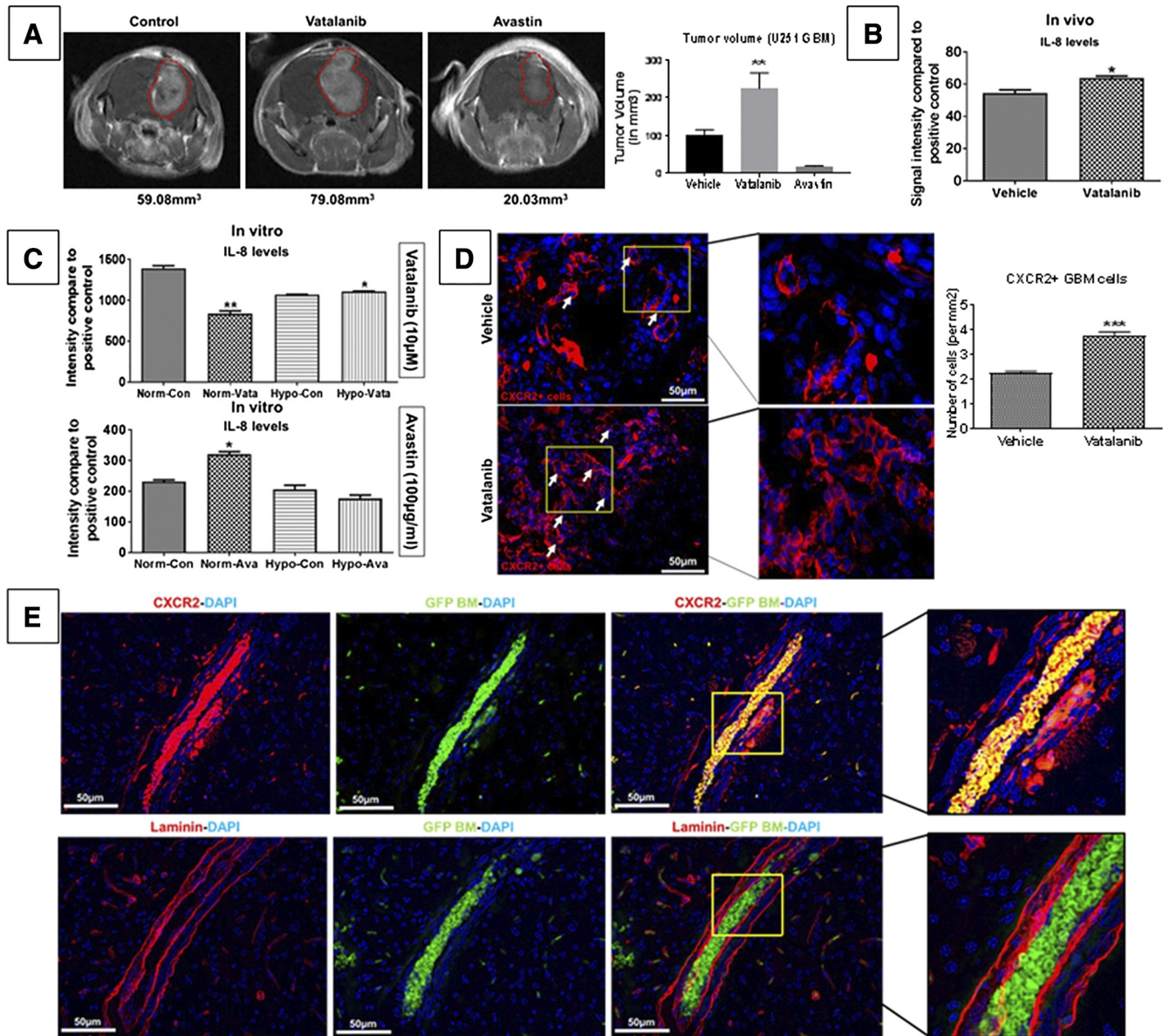
Figure 2. AAT increases the tumor burden, upregulates the IL-8 levels, and increases the numbers of CXCR2+ tumor cells that line the VM structures in GBM animal models. Quantitative data are expressed in mean ± SEM. *$P < .05$, **$P < .01$, and ***$P < .001$. (A) Representative MR images from vehicle ($n = 12$), vatalanib ($n = 16$), and avastin ($n = 5$) animal groups. The quantification of the tumor volume for these treatment groups is presented on the right. (B) Human cytokine array data showing upregulation of IL-8 levels *in vivo* and (C) *in vitro*. Representative immunofluorescence images showing (D) increased expression of CXCR2 (red) in vatalanib-treated tumors. (E) CXCR2+ GBM cells in the formation of VM structures in vatalanib-treated tumors. Scale = 50 µm. (F) Laminin and CXCR2 staining in vehicle- and avastin-treated groups and (G) CXCR2 and PAS staining in a rat model of U251 GBM showing increased numbers of CXCR2+ GBM cells lining PAS-positive VM structures in the early treatment vatalanib 0-21 and delayed treatment vatalanib 8-21 groups compared to vehicle-treated group ($n = 9$ per group); Scale = 50 µm. (H) BFP+ U251GBM (blue) cells as indicated by the white arrows incorporating into the host endothelial vascular structures (green) injected with Br1-GFP AAV; scale = 50 µm.
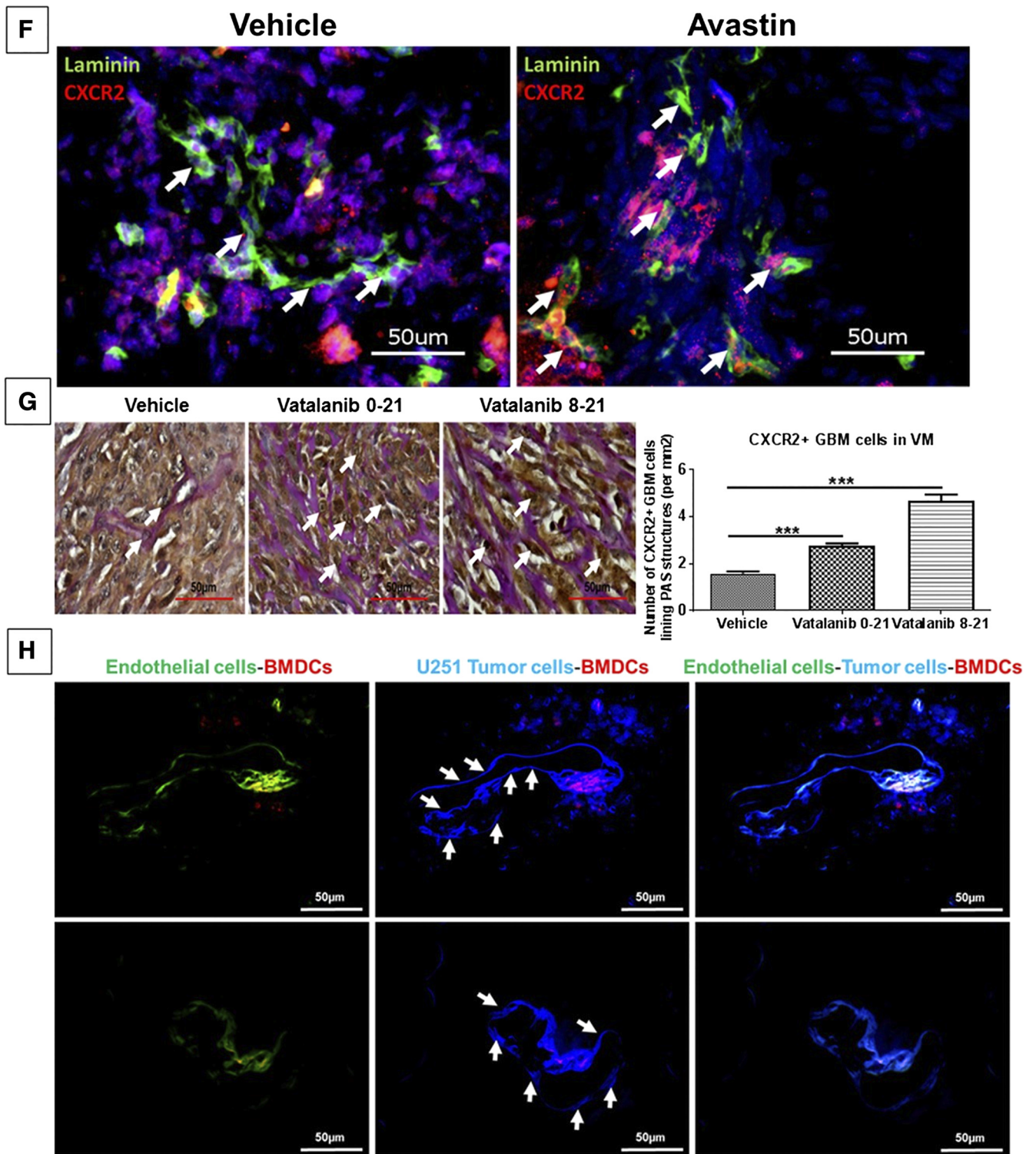
Figure 2 *(continued).*

#354230) incubated at 37°C for 1 hour. The tube formation was followed for 6 hours after treatment incubation with vehicle, vatalanib, avastin, and SB225002 in both normoxia and hypoxia conditions. The number of the complete tube-like networks without any breaks or disintegration was counted using Image J.

Statistical Analysis

Data were expressed in mean ± SEM unless otherwise stated. GraphPad Prism version 7.0 for Windows (GraphPad Software, Inc., San Diego, CA) was used to perform Student's *t* test. Any *P* value of less than .05 was considered significant.
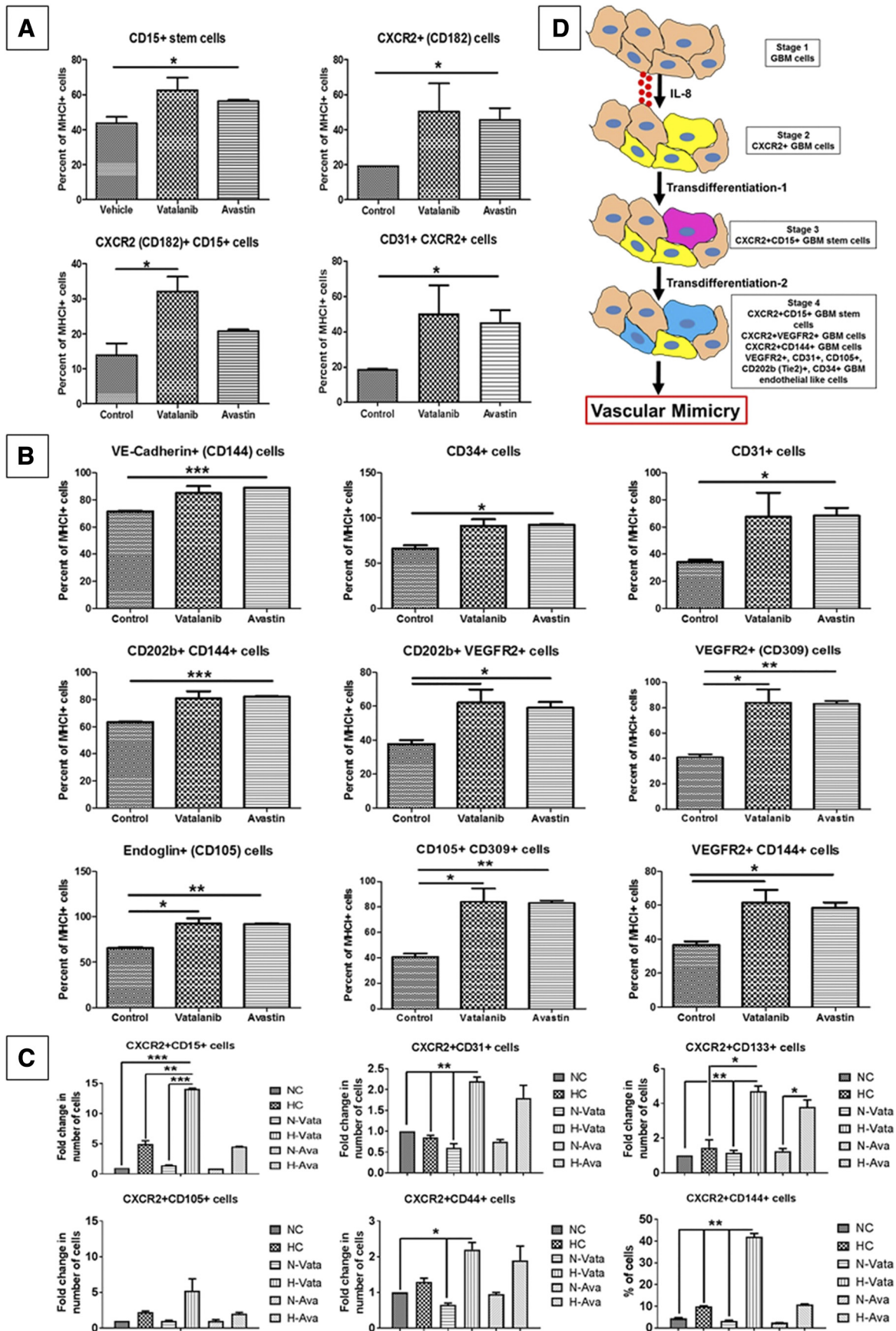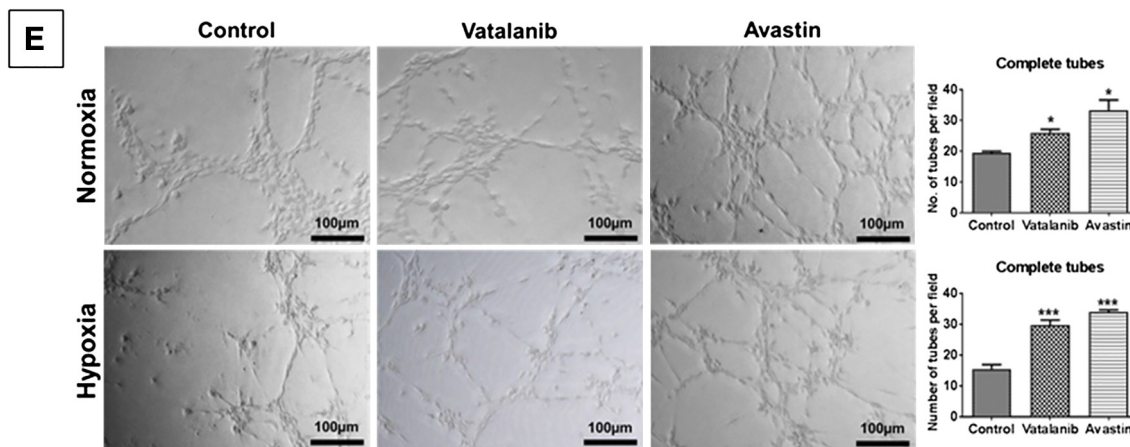
Figure 3. CXCR2+ tumor cells acquire endothelial and stem cell–like phenotypes following AAT. Quantitative data are expressed in mean ± SEM. *$P < .05$, **$P < .01$, and ***$P < .001$. $n = 3$. (A) Representative pictorial depiction of the acquisition of endothelial phenotypes by GBM cells. Flow cytometry data *in vivo* (B) showing different CXCR2 GBM subpopulations and (C) endothelial-like GBM subpopulations in the AAT-treated groups compared to the vehicle. (D) *In vitro* data showing CXCR2 GBM cells with endothelial cell–like and stem-like phenotypes following AAT treatment compared to control in hypoxic conditions for 24 hours. (E) U251 GBM cells treated with vehicle (control), vatalanib (10 μM), and avastin (100 μg/ml) and cultured in both normoxic (upper panel) and hypoxic (lower panel) conditions for 6 hours. Quantitative data are expressed in mean ± SEM. *$P < .05$ and ***$P < .001$.

Results

Clinical Relevance of IL-8, CXCR2, and VM Structures in Human GBM Samples

CXCR2 and PAS staining was performed on the microarray and GBM patient samples to ascertain the relevance of CXCR2+ GBM cells in human samples. We found that the CXCR2+ GBM cells lined the PAS-positive vascular structures in the higher-grade gliomas (Figure 1, A and B). To negate the possibility of the PAS staining as a random glycogen deposit, we stained GBM patient samples for vascular laminin and PAS and found that the PAS-positive structures were also positive for vascular laminin (Supplementary Figure S1). Next, 166 GBM samples were analyzed for IL-8 and CXCR2 genes from The Cancer Genome Atlas (TCGA) data to assess the overall survival and disease-free survival as a Kaplan-Meier estimate. We observed that there is a significantly poorer overall survival (log-rank test P value = .00948) and disease-free survival (log-rank test P value = .0108) in GBM samples with IL-8 and CXCR2 overexpression compared to GBM samples without IL-8 and CXCR2 overexpression (Figure 1C). We also correlated this finding with The VandenBoom brain data set. The data suggested that there is significantly increased CXCR2 expression in GBM compared to astrocytoma and mixed glioma samples (Figure 1D, *Brain and CNS cancer type*) and in recurrent cases ($n = 8$) compared to the primary tumor occurrence ($n = 8$) (Figure 1D, *Recurrence status*). Analysis of grade 2 ($n = 8$), grade 3 ($n = 4$), and grade 4 ($n = 4$) tumors revealed that the CXCR2 expression was significantly upregulated in grade 4 glioma cases when compared to the lower-grade glioma cases (Figure 1D, *GBM Grade*) [19]. We also observed that some of the CXCR2+ cells also have a lectin staining (white arrows) indicating that these GBM cells have acquired an endothelial-like phenotype (Figure 1E).

Effect of AAT on GBM Growth, IL-8, CXCR2+ Cells, and VM Structures in GBM Models

After confirming the importance of IL-8 and CXCR2 in the formation of VM in human GBM samples, we tested how VM contributes to therapy resistance in animal models of GBM. Animals bearing orthotopic U251 tumors were treated with vehicle, vatalanib, and avastin from day 8 to day 21 and then imaged with MRI. MRI identified significantly increased tumor growth in vatalanib-treated animals (Figure 2A). The quantification of the tumor volume for all the treatment groups is presented on the right of the MR images. No significant changes in the size of tumors treated with vatalanib and avastin were found in U87 GBM model (Supplementary Figure S2A).

Next, we found significant upregulation of IL-8 in the vatalanib-treated animals ($P < .05$) compared to the control group (Figure 2B). We then performed *in vitro* studies and observed significantly ($P < .05$) higher levels of IL-8 in the culture media when U251 cells were treated with vatalanib in hypoxic condition and with avastin in normoxic condition for 24 hours (Figure 2C).

To determine whether the AAT-treated tumors have an increased expression of CXCR2 in the tumor, we performed immunofluorescence staining with the hCXCR2 antibody on the vehicle- and vatalanib-treated tumors. The vatalanib-treated animals showed a higher number of CXCR2+ tumor cells ($P < .001$) compared to the vehicle-treated animals (Figure 2D). We found that CXCR2+ GBM cells lined the vascular structures in vatalanib-treated chimeric animal model [20] that carried the GFP-positive BMDCs and these tube-like structures were also lined with the vascular laminin, indicating that these structures were indeed functional in nature (Figure 2E). Further, to exclude the possibility of endogenous endothelial cell staining, we have labeled the human GBM cells implanted in athymic nude mice with CXCR2 antibody which has specificity to human CXCR2 antigen only and does not have cross-reactivity with mouse. Here, CXCR2+ GBM cells were shown to incorporate into tumor vasculature as confirmed by the laminin staining on the consecutive section from the same animal. Presence of red blood cells in the lumen indicates the functional status of the VM. We also found that there was no significant change in the overall laminin-positive areas in vehicle- and avastin-treated tumors, indicating inefficacy of avastin in disrupting VM structures (Figure 2F). Further, we found that the CXCR2+ GBM cells lining PAS-positive VM structures were
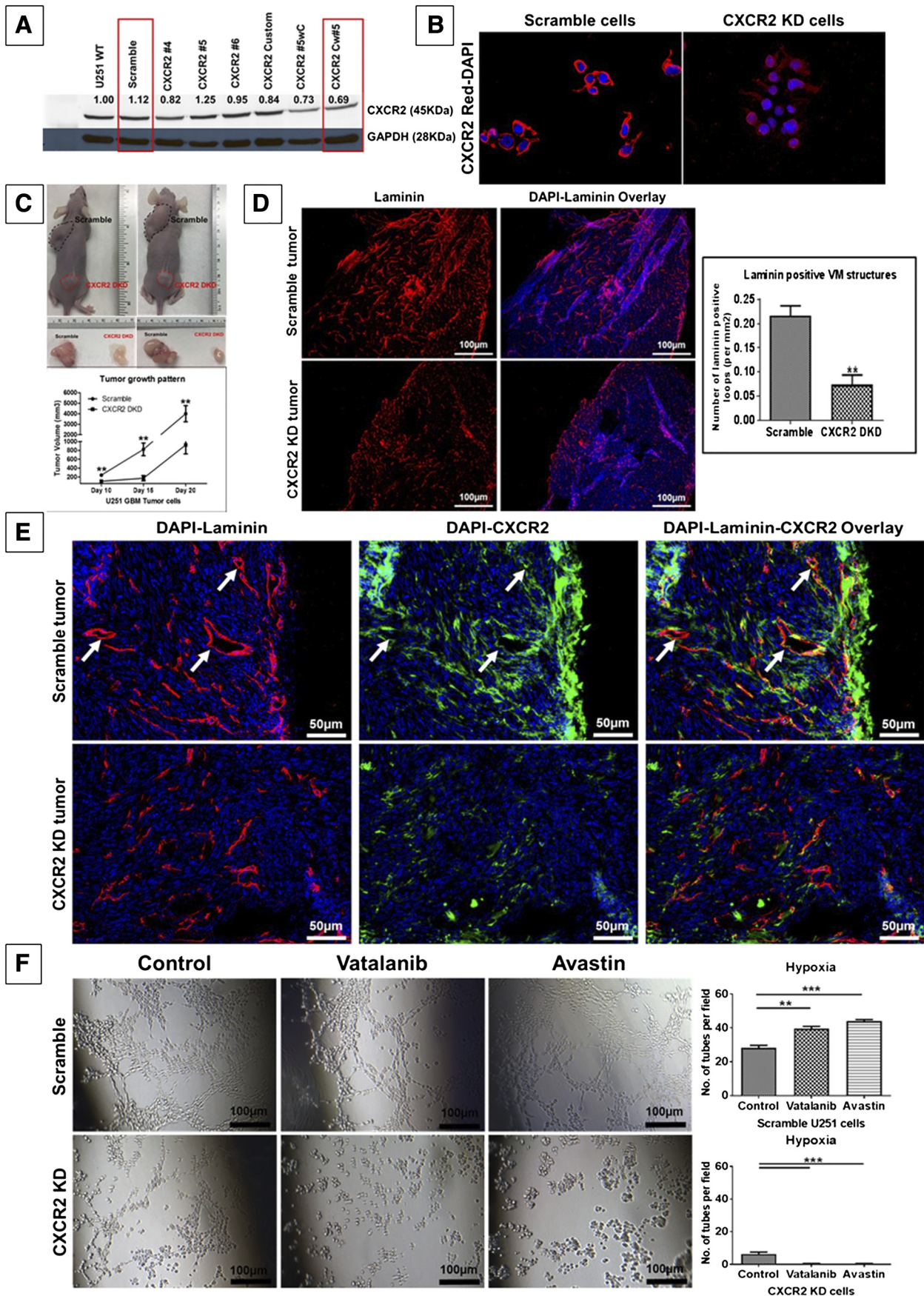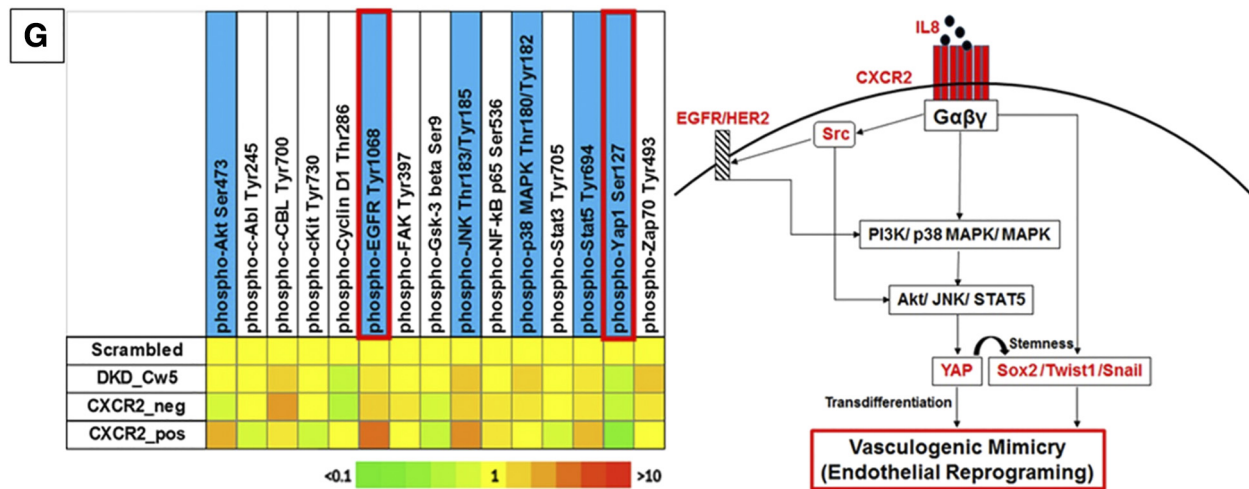
Figure 4. CXCR2-KD cells show significant overall decrease in tumor volume and form lesser laminin-positive VM structures. (A) Western blot with densitometry quantification and (B) immunofluorescence imaging showing the decreased expression CXCR2 in the CXCR2 knockdown cells (CXCR2 Cw#5) compared to scramble cells ($n = 2$). Representative images of (C) CXCR2-KD tumors showing significant reduction in the volume (five-fold) compared to scrambled tumors ($n = 4$). Immunofluorescence staining showing (D) reduction in the laminin-positive VM structures in the CXCR2-KD tumors compared to the scrambled tumors; scale = 100 μm. Quantitative data are expressed in mean ± SEM. **$P < .01$. (E) Absence of CXCR2+ GBM cells lining the laminin-positive structures in CXCR2-KD tumors; scale = 50 μm. (F) Scramble U251 and CXCR2 knockdown (CXCR2 DKD) U251 GBM cells were seeded on Matrigel for 6 hours in hypoxia. Quantitative data are expressed in mean ± SEM. *$P < .05$ and ***$P < .001$. (G) Differential expression patterns of phosphoproteins and proposed pathway schematic of IL8-CXCR2–mediated VM in GBM tumor cells.

significantly higher in both early and delayed vatalanib-treated groups ($P < .001$) compared to the control group (Figure 2G). In addition, we have generated a chimeric mouse model in which the endothelial cells in the brain were labeled with GFP using an AAV (Br1-GFP). DsRed bone marrow from donor was then engrafted into these mice. After successful engraftment of the bone marrow, BFP+ U251 GBM cells were implanted orthotopically into these animals. The incorporation of the blue GBM cells into the tumor vasculature can be noticed (Figure 2H). We also observed that both HF2303 and GBM811 PDX models also showed CXCR2+ GBM cells lining PAS-positive VM structures, indicating that CXCR2 GBM cell-mediated VM is a phenomenon that is present in human GBM samples, U251 *in vitro*, and PDX orthotopic glioma models (Supplementary Figure S2B).

CXCR2+ Tumor Cells Acquire Stem Cell–Like and Endothelial Phenotypes Following AAT

To identify whether AAT induces the upregulation of CXCR2+ GBM subpopulations with endothelial and stem cell–like properties, tumor cells from animals treated with AAT were analyzed by flow cytometry. We observed that both vatalanib- and avastin-treated groups showed a significant increase in CXCR2+ (CD182), CD15+, CXCR1+ (CD181), and CD31+ CXCR2+ endothelial-like cells ($P < .05$) compared to the control group (Figure 3A and Supplementary Figure S3A). Surprisingly, we noticed that the vatalanib- and avastin-treated tumors showed significant increase in other endothelial-like subpopulations ($P < .05$ to $P < .001$) compared to the control group. (Figure 3B). In U87 GBM model, we found a significant increase in CD309+ CD202b + and CD309+ CD144+ cells following vatalanib treatment, whereas no significant changes were observed in the CXCR2+, CXCR1+, CD15+, and CXCR2+ CD31+ populations. All the other endothelial cell–like populations showed a trend of decrease after treatment with avastin (Supplementary Figure S3, B and C). The representative FACS plots (from one animal from each treatment group) for the changes in the subpopulations of tumor cells following treatments with control,

vatalanib, and avastin are also included in the supplemental information section (Supplementary Figure S6, A, B, and C).

AAT Enhanced In Vitro GBM Cell-Derived Angiogenesis and Changed Phenotypes of GBM Cells

To identify the phenotypical characteristics of VM forming GBM cells, we performed flow cytometry using U251 cells treated with AAT *in vitro* cultured under normoxic and hypoxic conditions for 24 hours. We found two- to five-fold increase in CXCR2+ CD15+, CXCR2+ CD31+, CXCR2+ CD133+, CXCR2+ CD105+, CXCR2+ CD44+, and CXCR2+ CD144+ cells treated with vatalanib under hypoxic conditions and two- to four-fold increase in the CXCR2+ CD31+ and CXCR2+ CD133+ cells in the avastin-treated group under hypoxic conditions compared to the control cells (Figure 3C). A graphical representation of the transdifferentiation of the GBM cells into stem cell–like state and subsequent acquisition of endothelial phenotypes are represented (Figure 3D).

To assess the tube-forming capability of GBM cells, we performed *in vitro* Matrigel-based tube formation assay using U251 cells subjected to treatment with AAT. Surprisingly, AAT increased the number of complete tube-like VM structures on Matrigel in both normoxia ($P < .05$) and hypoxia ($P < .001$) after 6 hours of incubation compared to the control groups (Figure 3E). U87 cells were used under the aforementioned conditions as comparison (Supplementary Figure S3D).

CXCR2-KD Tumors Show Decreased Tumor Volume and VM

We utilized the shRNA-lentiviral system to knock down the expression of CXCR2 and observe whether the receptor has any effect on VM. The CXCR2-KD was confirmed using Western blotting and immunofluorescence staining (Figure 4, A and B). We observed that CXCR2-KD tumors were significantly ($P < .01$) smaller compared to the scrambled tumors throughout the study (Figure 4C). We repeated this experiment using an intracranial orthotopic model and also

confirmed the reduction in the tumor volume in the mice had CXCR2-KD tumors compared to the scrambled tumors (Supplementary Figure S4*A*).

With a knockdown efficiency of 40%-50%, CXCR2-KD tumors had significantly fewer and smaller laminin-positive structures ($P < .01$) compared to the scrambled tumors (Figure 4*D*). We further probed the scrambled and CXCR2-KD tumor samples with hCXCR2 antibody to determine whether there were any CXCR2+ GBM cells lining the laminin-positive structures. We repeated the experiment with an intracranial tumor model and observed that the CXCR2-KD tumors showed a reduction in the laminin and CXCR2 staining compared to the scrambled tumors (Supplementary Figure S4*A*). We found that CXCR2+ GBM cells were juxtaposing the laminin-positive vascular structures in the scrambled tumors. However, the CXCR2-KD tumors did not have CXCR2+ GBM cells lining their vascular laminin structures, indicating that CXCR2+ GBM cells play a crucial role in the formation of VM structures in GBM tumors (Figure 4*E* and Supplementary Figure S4*B*). Lectin-laminin and HIF-1α-laminin co-localization (Supplementary Figure S4*C*) was also observed in the scrambled tumors, indicating that these VM-like structures were indeed serving vascular purposes and that HIF-1α has a crucial role in mediating VM in the GBM tumors.

We found that CXCR2-KD cells have defective tube-forming capability compared to the scrambled cells in both normoxic (Supplementary Figure S4*D*) and hypoxic (Figure 4*F*) conditions with AAT. The total number of tube-like structures was significantly reduced with CXCR2-KD, and AAT did not restore or reverse the defective tube-forming capability of CXCR2-KD cells ($P < .001$) compared to scrambled cells.

Upon subjecting the scrambled, CXCR2-KD, CXCR2+ sorted, and CXCR2– sorted U251 cells for pathway analysis, significant reduction of p-EGFR Tyr1068 in the CXCR2-KD and CXCR2– cells was observed compared to the CXCR2+ sorted cells. CXCR2-KD and CXCR2– sorted cells showed increased phosphorylation of p-YAP1 compared to the CXCR2+ sorted cells. The hypothetical pathway and their contribution in VM have been proposed alongside (Figure 4*G* and Supplementary Figure S4*E*).

Intervening IL-8-CXCR2 Axis Decreases the Tumor Burden and CXCR2+ Endothelial Cell–Like and Stem Cell–Like Populations in GBM Tumors

Previously, we observed that HET0016 (a 20-HETE synthesis inhibitor) could dramatically reduce the levels of IL-8 in the U251 GBM animal model [18] and also reduce the incidence of VM [8]. U251 GBM-bearing animals were treated with vehicle, SB225002, and a combination of Vata+SB from day 8 to 21. We found decreased GBM growth in SB225002- and Vata+SB-treated mice compared to the control group (Figure 5*A*). The quantification of the tumor volume for all the treatment groups is presented on the right of the MR images.

Since we identified an increase in the CXCR2+ GBM tumor cells after AAT with endothelial and stem cell–like characteristics, we believed that these novel CXCR2+ subpopulations were responsible for mediating the AAT resistance in GBM. Moreover, we hypothesized that SB225002 would reduce these novel subpopulations. As expected, CXCR2+, CD15+, CXCR2+ CD15+, CXCR2+ CD31+, CXCR1+, and CXCR1+ CXCR2+ cells showed a significant reduction in numbers compared to the vehicle- and AAT-treated

group (Figure 5*B* and Supplementary Figure S5*A*). In addition, we noticed a significant decrease in the endothelial-like subpopulations compared to the vehicle- and AAT-treated groups (Figure 5*C*). The representative FACS plots (from one animal from each treatment group) for the changes in the subpopulations of tumor cells following treatments with control, SB225002, and Vata+SB are also included (Supplementary Figure S7, *A*, *B*, and *C*).

Next, we observed that SB225002 significantly disrupted the tube-forming capability of U251 cells in normoxic and hypoxic conditions compared to the control groups (Figure 5*D* and Supplementary Figure S5*B*). We also investigated whether SB225002 and Vata+SB could reduce the total CXCR2+ cells lining the laminin-positive VM structures and found that both SB225002 and the Vata+SB reduced the laminin-positive VM structures compared to vehicle-treated group (Figure 5*E*).

Discussion

Here, we report that CXCR2-positive tumor cells contribute to the PAS-positive VM structures in human GBM tumor samples. The CXCR2+ GBM cells acquire the lectin marker indicating an acquisition of the endothelial phenotype by these cells. Also, with the progression of the glioma from lower grades to higher, there is an increased number of PAS-positive structures lined by CXCR2+ GBM cells. The van den Boom brain Oncomine data analysis also showed a positive correlation between CXCR2 expression and the recurrence status and grade of GBM. IL-8– and CXCR2-overexpressing GBM tumors also showed a poorer overall survival and disease-free survival on a Kaplan-Meier estimate. Moreover, Yang et al. reported that an increased CXCR2 expression was correlated with abysmal prognosis, a higher grade of tumor, and recurrence in human glioma patient samples [21]. While investigating the mechanisms of acquired therapy resistance in GBM, we observed that AAT caused a paradoxical increase in the tumor burden and upregulated the IL8 levels and the CXCR2 expression on U251 GBM cells in a mouse model. We focused on IL-8-CXCR2 axis because of its significant role in maintaining stemness compared to CXCR1 that is primarily responsible for mitogenic activity. IL8-CXCR2–upregulated tumor cells were able to form functional VM structures in the tumor tissue. Reports have underlined the role of IL-8 in facilitating invasion in gliomas through NF-κB pathway [22], worsening of tumor grade in astrocytic neoplasms [23], and increasing the apoptotic threshold and sprouting potential of tumor-associated endothelial cells (ECs) [24,25]. Recent studies have shown that avastin failed to recapitulate the disruptive effect of VEGFR2 inhibitor (SU1498) on tube-forming capability of U87 cells [26]. We demonstrated that the tube-forming capability of U251 and U87 cells was accelerated on Matrigel following the treatment of both VEGFR2 blocker (vatalanib) and VEGF-A ligand-neutralizing antibody (avastin). In addition, it has been reported that SB225002 (CXCR2 inhibition) disrupts the tube formation of human umbilical vein endothelial cells seeded either independently or in co-culture with tumor cells (HPDE-Kras) [27,28].

Interestingly, when we analyzed the CXCR2-KD and CXCR2– U251 sorted cells, we observed a decrease of p-EGFR Tyr1068 levels in the CXCR2-KD and CXCR2– cells compared to the CXCR2+ U251 sorted cells. Given the significance of EGFR gene amplification in primary GBM [29] and the role of EGFR and EGFRvIII in GBM invasion and angiogenesis [30,31], our findings emphasize the importance of the EGFR and further nominate CXCR2 as an interesting therapeutic target to control GBM growth. In addition to
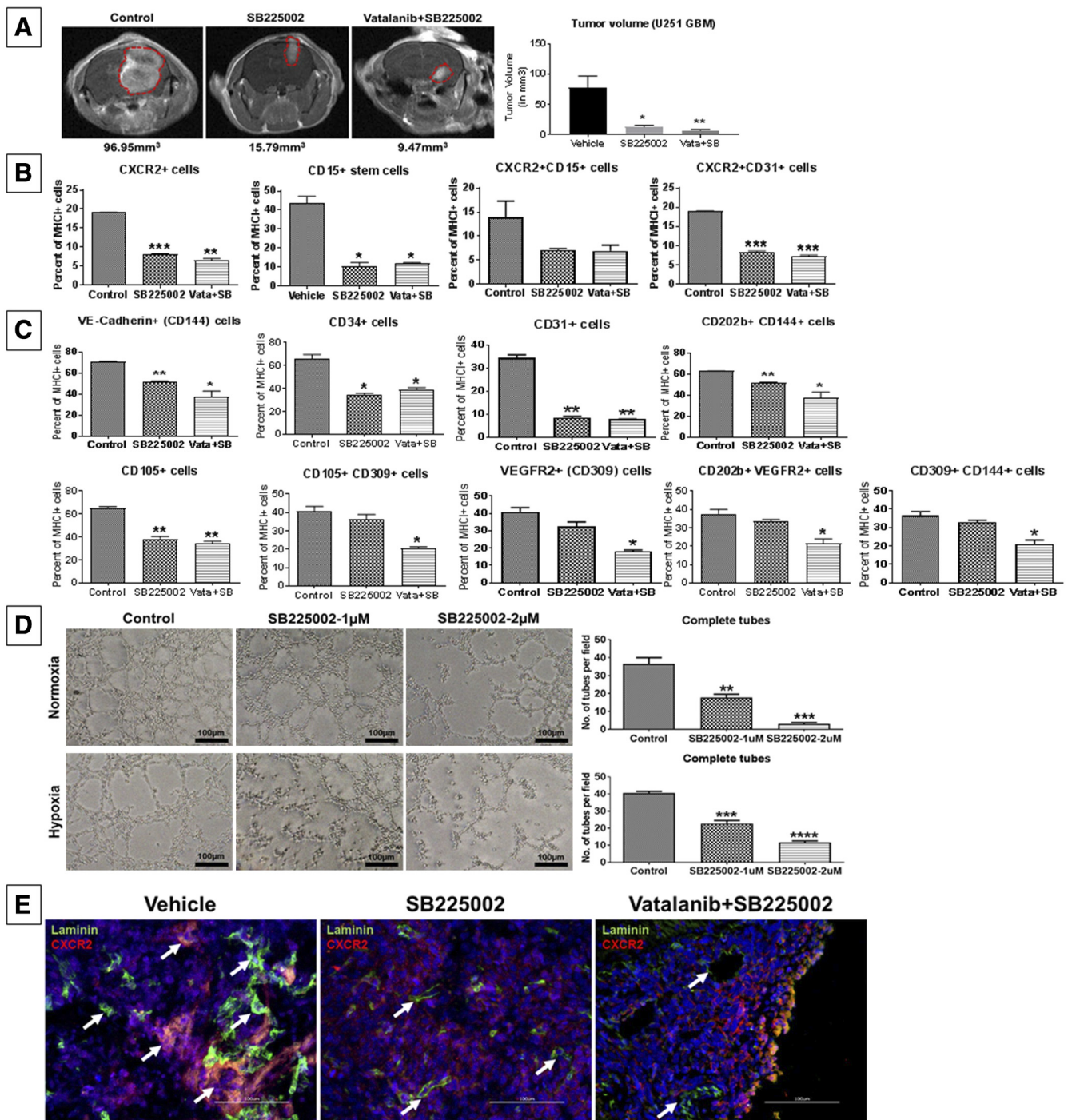
Figure 5. SB225002 therapy decreases the tumor burden and CXCR2+ endothelial cell-like and stem cell–like populations in GBM tumors. Quantitative data are expressed in mean ± SEM. *P < .05, **P < .01, and ***P < .001. n = 3. (A) Representative MR images from vehicle, SB225002, and vatalanib + SB225002 animal groups. The quantification of the tumor volume for these treatment groups is presented on the right. Flow cytometry data *in vivo* (B) showing different CXCR2 GBM subpopulations and (C) endothelial-like GBM subpopulations in vehicle, SB225002, and vatalanib + SB225002 animal groups. (D) U251 GBM cells treated with vehicle (control) and two different concentrations of SB225002 (1 μM and 2 μM) and cultured in both normoxic (upper panel) and hypoxic (lower panel) conditions for 6 hours. Quantitative data are expressed in mean ± SEM. *P < .05 and ***P < .001. (E) Representative images of the areas within the tumor showing decreased expression of CXCR2+ GBM cells and vascular laminin coverage compared to the vehicle-treated groups, n = 3.

this, increased phosphorylation of p-YAP1 Ser127 was observed in CXCR2-KD and CXCR2– U251 sorted cells compared to the CXCR2+ U251 cells. Recent studies have demonstrated the role of YAP1 in maintaining stem cell–like state and VM in non–small cell lung cancer. Inhibiting or depleting YAP1 suppressed self-renewal

and VM of stem-like cells [32]. It would be interesting to look into the role of YAP1 in IL-8-CXCR2 axis-mediated VM in GBM. A proposed model of AAT-mediated resistance through VM and the use of CXCR2 inhibitor SB225002 to counter the AAT therapy resistance by decreasing the acquisition of stem cell–like and
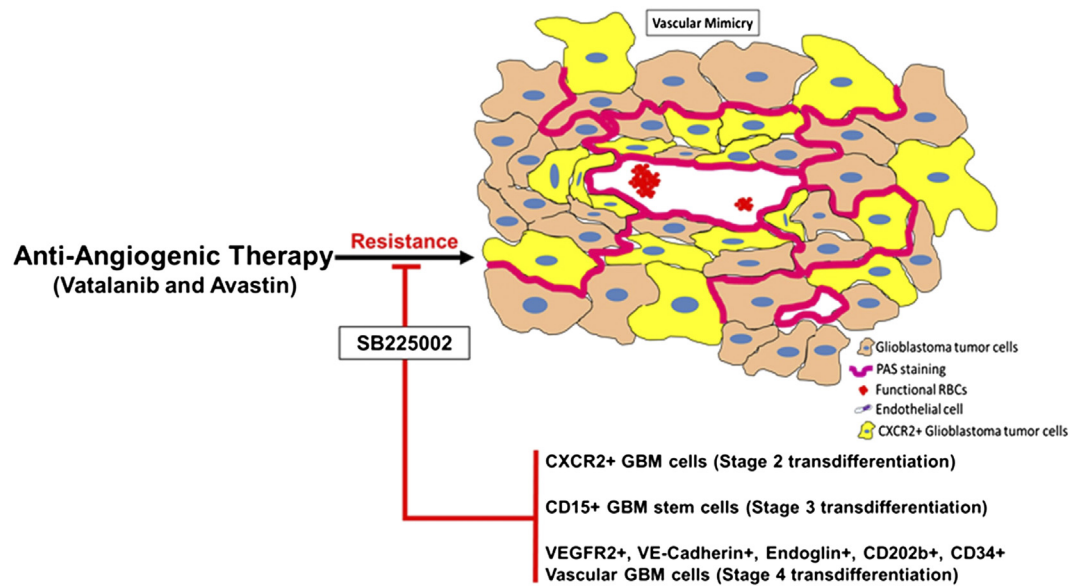
Figure 6. Proposed schematic of the acquisition of VM-mediated therapy resistance to AAT and intervention using SB225002.

endothelial cell–like phenotypes in CXCR2+ GBM cells is shown in Figure 6.

Endothelial phenotype acquisition of the tumor cells has already been established as a key feature in the formation of VM structures in the tumors [12,33]. We originally reported in this study that CXCR2+ GBM cells acquire stem cell–like and endothelial phenotypes following AAT both *in vitro* and *in vivo*, strengthening our hypothesis that CXCR2+ GBM cells drive the AAT resistance *via* VM. Recently, utilization of IL-8-CXCR2 pathway disrupting agents showed an inhibition of cell growth and drug resistance [34] and an improvement in the antitumorigenic and anti-AAT responses [28]. In our current study, SB225002 was able to inhibit tube formation in both normoxic and hypoxic conditions. Surprisingly, treatment with SB225002 and Vata+SB decreased CXCR2+ endothelial-like and stem cell–like subpopulations in U251 GBM mouse model compared to the AAT-treated groups. A recent study has reported that SB225002 could decrease proliferation, impair vasculogenic mimicry formation, and block the uptake of IL-8 in breast cancer through downregulation of transgelin [35]. However, our current study establishes VM as a mechanism of therapeutic resistance in AAT and further describes the CXCR2+ GBM cells with endothelial like-phenotypes following AAT. Further, both SB225002 and Vata+SB significantly reduced these populations, thereby strengthening the use of SB225002 as an adjuvant to AAT or other chemotherapeutic approaches.

We report that CXCR2-KD tumors showed significantly decreased tumor volume and reduction in the laminin-positive VM structures *in vivo*. This laminin-positive VM structures could be clearly seen as poorly developed vascular structures, and there is an absence of the CXCR2+ GBM cells in the lining of these structures in the CXCR2-KD tumors.

In conclusion, we have provided solid evidence for the involvement of IL-8-CXCR2 pathway in the formation of VM structures and mediating AAT resistance in human GBM tumors and animal models. SB225002 can successfully impede the IL-8-CXCR2 pathway to prevent VM and thus open new avenues for the consideration of these drugs as adjuvants to current therapies to treat therapy-resistant or recurrent GBMs.

Supplementary data to this article can be found online at https://doi.org/10.1016/j.neo.2018.08.011.

Conflict of Interest

The authors declare no potential conflicts of interest.

Author Contributions

Kartik Angara and Thaiz Borin: conceptualization, data curation, formal analysis, investigation, methodology, writing (original draft); Bhagelu Achyut and Ali S. Arbab: project administration, resources, supervision, funding acquisition, writing (review and editing); Mohammad H. Rashid, Roxan Ara, Ping-Chang Lin, and A. S. M. Iskander: methodology, data curation, formal analysis; Iryna Lebedyeva and Roni J. Bollag: resources, software.

References

[1] Remer S and Murphy ME (2004). The challenges of long-term treatment outcomes in adults with malignant gliomas. *Clin J Oncol Nurs* **8**, 368–376.

[2] Los M, Roodhart JM, and Voest EE (2007). Target practice: lessons from phase III trials with bevacizumab and vatalanib in the treatment of advanced colorectal cancer. *Oncologist* **12**, 443–450.

[3] Norden AD, Drappatz J, and Wen PY (2008). Novel anti-angiogenic therapies for malignant gliomas. *Lancet Neurol* **7**, 1152–1160.

[4] Dietrich J, Norden AD, and Wen PY (2008). Emerging antiangiogenic treatments for gliomas - efficacy and safety issues. *Curr Opin Neurol* **21**, 736–744.

[5] Bergers G and Hanahan D (2008). Modes of resistance to anti-angiogenic therapy. *Nat Rev Cancer* **8**, 592–603.

[6] Jain RK, di Tomaso E, Duda DG, Loeffler JS, Sorensen AG, and Batchelor TT (2007). Angiogenesis in brain tumours. *Nat Rev Neurosci* **8**, 610–622.

[7] de Vries NA, Beijnen JH, Boogerd W, and van Tellingen O (2006). Blood-brain barrier and chemotherapeutic treatment of brain tumors. *Expert Rev Neurother* **6**, 1199–1209.

[8] Angara K, Rashid MH, Shankar A, Ara R, Iskander A, Borin TF, Jain M, Achyut BR, and Arbab AS (2017). Vascular mimicry in glioblastoma following anti-angiogenic and anti-20-HETE therapies. *Histol Histopathol* **32**, 917–928.

[9] El Hallani S, Boisselier B, Peglion F, Rousseau A, Colin C, Idbaih A, Marie Y, Mokhtari K, Thomas JL, and Eichmann A, et al (2010). A new alternative mechanism in glioblastoma vascularization: tubular vasculogenic mimicry. *Brain* **133**, 973–982.

[10] Mao JM, Liu J, Guo G, Mao XG, and Li CX (2015). Glioblastoma vasculogenic mimicry: signaling pathways progression and potential anti-angiogenesis targets. *Biomark Res* **3**, 8.

[11] Maniotis AJ, Folberg R, Hess A, Seftor EA, Gardner LM, Pe'er J, Trent JM, Meltzer PS, and Hendrix MJ (1999). Vascular channel formation by human melanoma cells in vivo and in vitro: vasculogenic mimicry. *Am J Pathol* **155**, 739–752.

[12] Ricci-Vitiani L, Pallini R, Biffoni M, Todaro M, Invernici G, Cenci T, Maira G, Parati EA, Stassi G, and Larocca LM, et al (2010). Tumour vascularization via endothelial differentiation of glioblastoma stem-like cells. *Nature* **468**, 824–828.

[13] Folberg R and Maniotis AJ (2004). Vasculogenic mimicry. *APMIS* **112**, 508–525.

[14] Vartanian AA (2012). Signaling pathways in tumor vasculogenic mimicry. *Biochemistry (Mosc)* **77**, 1044–1055.

[15] Clemente M, Perez-Alenza MD, Illera JC, and Pena L (2010). Histological, immunohistological, and ultrastructural description of vasculogenic mimicry in canine mammary cancer. *Vet Pathol* **47**, 265–274.

[16] Angara K, Borin TF, and Arbab AS (2017). Vascular mimicry: a novel neovascularization mechanism driving anti-angiogenic therapy (AAT) resistance in glioblastoma. *Transl Oncol* **10**, 650–660.

[17] Soda Y, Myskiw C, Rommel A, and Verma IM (2013). Mechanisms of neovascularization and resistance to anti-angiogenic therapies in glioblastoma multiforme. *J Mol Med* **91**, 439–448.

[18] Jain M, Gamage NH, Alsulami M, Shankar A, Achyut BR, Angara K, Rashid MH, Iskander A, Borin TF, and Wenbo Z, et al (2017). Intravenous formulation of HET0016 decreased human glioblastoma growth and implicated survival benefit in rat xenograft models. *Sci Rep* **7**, 41809.

[19] van den Boom J, Wolter M, Kuick R, Misek DE, Youkilis AS, Wechsler DS, Sommer C, Reifenberger G, and Hanash SM (2003). Characterization of gene expression profiles associated with glioma progression using oligonucleotide-based microarray analysis and real-time reverse transcription-polymerase chain reaction. *Am J Pathol* **163**, 1033–1043.

[20] Achyut BR, Shankar A, Iskander AS, Ara R, Knight RA, Scicli AG, and Arbab AS (2016). Chimeric mouse model to track the migration of bone marrow derived cells in glioblastoma following anti-angiogenic treatments. *Cancer Biol Ther* **17**, 280–290.

[21] Yang L, Liu Z, Wu R, Yao Q, Gu Z, and Liu M (2015). Correlation of C-X-C chemokine receptor 2 upregulation with poor prognosis and recurrence in human glioma. *OncoTargets Ther* **8**, 3203–3209.

[22] Raychaudhuri B and Vogelbaum MA (2011). IL-8 is a mediator of NF-kappaB induced invasion by gliomas. *J Neuro-Oncol* **101**, 227–235.

[23] Van Meir E, Ceska M, Effenberger F, Walz A, Grouzmann E, Desbaillets I, Frei K, Fontana A, and de Tribolet N (1992). Interleukin-8 is produced in neoplastic and infectious diseases of the human central nervous system. *Cancer Res* **52**, 4297–4305.

[24] Brat DJ, Bellail AC, and Van Meir EG (2005). The role of interleukin-8 and its receptors in gliomagenesis and tumoral angiogenesis. *Neuro Oncol* **7**, 122–133.

[25] Li A, Dubey S, Varney ML, Dave BJ, and Singh RK (2003). IL-8 directly enhanced endothelial cell survival, proliferation, and matrix metalloproteinases production and regulated angiogenesis. *J Immunol* **170**, 3369–3376.

[26] Francescone R, Scully S, Bentley B, Yan W, Taylor SL, Oh D, Moral L, and Shao R (2012). Glioblastoma-derived tumor cells induce vasculogenic mimicry through Flk-1 protein activation. *J Biol Chem* **287**, 24821–24831.

[27] Matsuo Y, Campbell PM, Brekken RA, Sung B, Ouellette MM, Fleming JB, Aggarwal BB, Der CJ, and Guha S (2009). K-Ras promotes angiogenesis mediated by immortalized human pancreatic epithelial cells through mitogen-activated protein kinase signaling pathways. *Mol Cancer Res* **7**, 799–808.

[28] Devapatla B, Sharma A, and Woo S (2015). CXCR2 inhibition combined with sorafenib improved antitumor and antiangiogenic response in preclinical models of ovarian cancer. *PLoS One* **10**e0139237.

[29] Fuller GN and Bigner SH (1992). Amplified cellular oncogenes in neoplasms of the human central nervous system. *Mutat Res* **276**, 299–306.

[30] Penar PL, Khoshyomn S, Bhushan A, and Tritton TR (1997). Inhibition of epidermal growth factor receptor-associated tyrosine kinase blocks glioblastoma invasion of the brain. *Neurosurgery* **40**, 141–151.

[31] Bonavia R, Inda MM, Vandenberg S, Cheng SY, Nagane M, Hadwiger P, Tan P, Sah DW, Cavenee WK, and Furnari FB (2012). EGFRvIII promotes glioma angiogenesis and growth through the NF-kappaB, interleukin-8 pathway. *Oncogene* **31**, 4054–4066.

[32] Bora-Singhal N, Nguyen J, Schaal C, Perumal D, Singh S, Coppola D, and Chellappan S (2015). YAP1 regulates OCT4 activity and SOX2 expression to facilitate self-renewal and vascular mimicry of stem-like cells. *Stem Cells* **33**, 1705–1718.

[33] Wang R, Chadalavada K, Wilshire J, Kowalik U, Hovinga KE, Geber A, Fligelman B, Leversha M, Brennan C, and Tabar V (2010). Glioblastoma stem-like cells give rise to tumour endothelium. *Nature* **468**, 829–833.

[34] Sharma B, Varney ML, Saxena S, Wu L, and Singh RK (2016). Induction of CXCR2 ligands, stem cell-like phenotype, and metastasis in chemotherapy-resistant breast cancer cells. *Cancer Lett* **372**, 192–200.

[35] Aikins AR, Kim M, Raymundo B, and Kim CW (2017). Downregulation of transgelin blocks interleukin-8 utilization and suppresses vasculogenic mimicry in breast cancer cells. *Exp Biol Med* **242**, 573–583.